Alternative choices of Coulomb channel functions

R. Guérout,[1] Ch. Jungen,[1,2,*] H. Oueslati,[1,3] S. C. Ross,[4,5] and M. Telmini[3]
[1]*Laboratoire Aimé Cotton du CNRS, Bâtiment 505, Université de Paris-Sud, F-91405 Orsay, France*
[2]*Department of Physics and Astronomy, University College London, London WC1E 6BT, United Kingdom*
[3]*LSAMA, Department of Physics, Faculty of Sciences of Tunis, University of Tunis, El Manar, 2092 Tunis, Tunisia*
[4]*Department of Physics, University of New Brunswick, P.O. Box 4400, Fredericton, New Brunswick, Canada E3B 5A3*
[5]*Infrared Free Electron Laser Research Center, Tokyo University of Science, 2641 Yamazaki, Noda Chiba, 278–8510, Japan*
(Received 3 March 2009; published 29 April 2009)

A class of Coulomb radial functions is defined for use in atomic or molecular Rydberg multichannel quantum-defect calculations. The associated accumulated radial phase parameters $\beta(\epsilon)$ have a simple functional dependence on the energy, analogous to the familiar Rydberg relation where $\beta(\epsilon)=\pi(n^*-l)$, with $n^*=(-\epsilon)^{-1/2}$, enabling easy use in the empirical fitting of complex multichannel spectra. However, "false roots" at low-energy and strong energy dependences of the quantum defects are largely avoided in the approach, which also may be implemented in the framework of *ab initio* R-matrix calculations in a straightforward manner. The method is illustrated with one-channel and multichannel examples relating to atomic potassium, nitric oxide, and molecular hydrogen.

DOI: 10.1103/PhysRevA.79.042717 PACS number(s): 03.65.Nk, 34.10.+x

I. INTRODUCTION

The power of the Rydberg equation resides in the fact that it provides a description of a whole family of atomic or molecular electronic excited states—a Rydberg series—in compact form in terms of a single parameter, the quantum defect. The generalization of the Rydberg equation, known as the multichannel quantum-defect theory (MQDT), achieves this for an arbitrary number of coupled series of Rydberg states (see [1] for references). Electronic Rydberg states arise when a single atomic or molecular electron is excited into an orbit that is situated mostly outside the positively charged residual ion core. The quantum defect—or each individual element of the quantum-defect matrix in the multichannel case—is typically nearly constant or varies slightly and smoothly along a given series. It extrapolates smoothly across the ionization threshold into the electronic continuum where it turns into the electron scattering phase shift measured in units of π radians. A Rydberg series and the adjoining ionization continuum are therefore considered together as a "Rydberg channel."

The constancy or near constancy of the quantum defect has various implications which contribute to the success of quantum-defect theory (QDT). Interpolations and extrapolations of quantum-defect matrix elements enable one to infer scattering (continuum) phase shifts from bound-state spectroscopic data. Calculations of quantum-defect parameters from first principles may be carried out on a coarse energy mesh thus enhancing the efficiency of *ab initio* codes. In molecular applications the success of the frame transformation method to account for rovibronic interactions hinges on a weak energy dependence of the clamped-nuclei quantum defects (see references given in [1]).

Quantum-defect theory however is plagued by recurrent problems occurring in the bound energy range at low energies where the Rydberg spectrum connects to the valence state region and Rydberg channels are said to become "strongly closed." In molecules where the orbital angular momentum l of the Rydberg electron is not in general a sharply defined quantity, it is often not clear how a Rydberg series terminates at its lower end. Indeed, "spurious" or "false" solutions occur quite often in quantum-defect calculations in the strongly closed range, and unfortunately they cannot always be recognized easily as such. Seaton [2] therefore recommended that QDT, in its most common form, "should be restricted to energies ϵ such that $\epsilon \geq -1/l^2$," i.e., to "weakly closed" channels. In multichannel problems, however, strongly closed channels often coexist with weakly closed channels at a given energy. Further, in molecules a channel which is weakly closed for one nuclear geometry may become strongly closed for another. It therefore appears desirable to include the strongly closed channels along with the Rydberg manifold—this approach has been applied with success, e.g., to the $^1\Sigma_g^+$ double minimum states of H_2 which have half-Rydberg and half-valence state characters [3,4]. Mulliken [5], in a similar context, although without referring to quantum-defect theory, coined the expression "Rydbergization" for valence states which turn adiabatically into Rydberg states [6]. His ideas in fact go back to the 1920s when he introduced the closely related concept of "promoted electrons" [7].

The appearance of "spurious" solutions predicted by the Rydberg equation lower than the lowest true bound state of a series is probably the most obvious problem arising in the strongly closed range. While in a one-channel situation such spurious solutions can sometimes be eliminated by inspection, they may lead to unphysical channel interactions affecting the true states as well [8]. In 1979, Greene [9] published an insightful paper, in which he presented a discussion of the energy dependences to be expected for atomic quantum defects in general. From this paper, which has unjustly received only limited attention, it becomes apparent that false roots occur when the energy dependence of the quantum defect

*Corresponding author; christian.jungen@lac.u-psud.fr

has been neglected or when it has not been taken into account correctly, e.g., by inappropriate extrapolation.

Greene's work also showed that as the energy gets very far below the ionization potential, both the quantum defect and the total accumulated radial phase of the Rydberg wave function should approach zero. This may be appreciated by considering the familiar atomic Rydberg quantization rule,

$$\mu + n^* - l = n(n \text{ positive integer}),$$

$$\epsilon = -\frac{1}{n^{*2}} = -\frac{1}{(n+l-\mu)^2}, \tag{1}$$

in which n^* is the effective principal quantum number, l is the orbital angular momentum, μ is the quantum defect, and ϵ is the energy in Rydberg units. The integer n is the number of radial lobes of the Rydberg wave function corresponding to the number of radial nodes minus one. The significance of the top line of Eq. (1) is that it decomposes the total phase of the radial wave function into two portions: $\pi\mu$ is the radial phase accumulated inside the core while $\pi(n^*-l)$ is that portion accumulated in the asymptotic Coulomb region. The quantity

$$\beta = \pi(n^* - l) \tag{2}$$

is defined continuously for every energy and is called the "accumulated phase parameter." The two contributions must add up to an integer times π in order for a bound quantum state to exist. Of course, the lower one goes in energy, the less phase accumulates. Therefore in the strongly closed limit no phase accumulates at all. That is, in the limit $\epsilon \to -\infty$, we have $\beta + \pi\mu \to 0$ so that $-\mu \to n^* - l$, the accumulated phase factor. Greene pointed out that even before reaching this extreme limit, false roots of Eq. (2) must occur unless the quantum defect drops away from a constant value. In fact it tends to "cling" [9] to $-(n^*-l)$, evolving closely parallel to it at low energy. This behavior is discernible in the plot of Fig. 1, where for n^* below about 1, the $0-\mu$ curve matches the n^*-l curve. The same limiting effect can be seen in Fig. 7 for the base pair defined in this paper although only at lower energies.

These arguments, and Eq. (1) in particular, reveal the fact that the quantum defect not only provides information about the bound-state energies but also about the radial Rydberg wave functions. Indeed, in QDT the radial wave function emerging from the core $(r < r_c)$ into the asymptotic region $(r > r_c)$ is written in scattering form in terms of the quantum defect μ:

$$\psi_l(r > r_c) = f_l(r)\cos\ \pi\mu_l - g_l(r)\sin\ \pi\mu_l, \tag{3}$$

where f_l and g_l are the regular and irregular Coulomb functions analogous to the sin-type and cos-type functions used in the continuum. From Eq. (3) it becomes further apparent that the value of the quantum defect μ depends on how $f_l(r)$ and $g_l(r)$ are defined at $r = r_c$ where $\psi(r)$ matches to the function inside the core. Indeed, we shall see below that we can work with an infinite variety of Coulomb base pairs, each of which has its own (usually energy dependent) quantum defect. The forms of Eqs. (1) and (2) are specific to the base pair called (s,c) by Seaton.

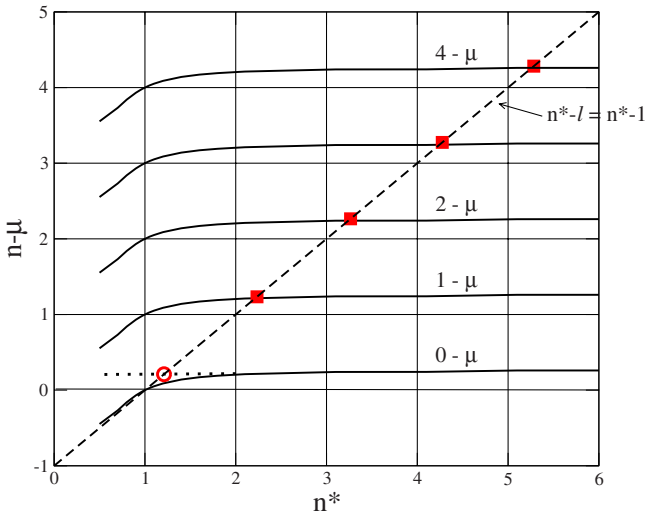

FIG. 1. (Color online) ^2P np series in potassium: the quantity $n-\mu$ is plotted versus the effective principal quantum number n^* for each of $n=0$ to 4. The full lines correspond to $n-\mu$ with n integer and μ as calculated in Sec. IV A. The dashed diagonal line corresponds to $n^*-l=n^*-1$, here, with n^* interpreted as a continuous parameter [see Eq. (1)]. Bound states occur each time the broken-line curve crosses one of the full lines. Full squares: observed values. Open circle: false root. (cf. the text for details).

The familiar R-matrix-type matching condition of short-range and asymptotic functions (written here in one-channel form for convenience and omitting the channel indices l) reads as [10]

$$\tan\ \pi\mu = \left[\frac{W(\psi,f)}{W(\psi,g)}\right]_{r=r_c} \equiv \frac{f}{g}\left[\frac{\frac{f'}{f} - \frac{\psi'}{\psi}}{\frac{g'}{g} - \frac{\psi'}{\psi}}\right]_{r=r_c}. \tag{4}$$

In this expression primes refer to the derivative with respect to the radial coordinate r and ψ represents the exact wave function that reflects the full Hamiltonian and which is matched to the base pair at the edge of the core. For r values well beyond the core radius Eq. (4) will be independent of the matching radius r_c, but it remains in principle energy dependent. It is thus clear that the evolution of the quantum defects with energy, in particular in the strongly closed regime, is intimately connected with the way the base pair (f_l, g_l) of Coulomb functions has been normalized. This again is a point which clearly emerges from Ref. [9], but which has been overlooked in some of the more recent work.

Indeed, these problems are not new, and a substantial number of papers has been devoted to their discussion in the past. Ham [11] defined a base pair of Coulomb functions, commonly called (f,h) with associated quantum defects "η," which in many cases helps to avoid false solutions in strongly closed channels and reputedly yields a smoother energy dependence for the quantum defects. Among recent papers dealing with the Coulomb problem we mention the

work of Gorczyca and Badnell [12] and of Child and Hiyama [13]. Numerical approaches based on Milne's [14] phase-amplitude theory, while remaining applicable to Coulomb fields, generalize QDT to asymptotic potentials of arbitrary shape [15,16]. They do not produce false roots generally, but the analytical simplicity of the Rydberg equation is lost.

The present work builds on these earlier achievements in an effort to further clarify the connection between the Coulomb basis pair used and the energy dependence of the corresponding quantum defects, as well as the occurrence of false roots. In this paper we propose a type of Coulomb base pair which we shall denote as "energy modified." These have enough built-in flexibility to enable one to deal with strongly-closed channels in a satisfactory manner. One of our primary goals is to retain the basic advantage of Eq. (1), which is that the accumulated phase parameter $\beta(\epsilon)=\pi(n^*-l)$ is related to the energy ϵ by a simple algebraic expression [the Rydberg equation in the case of Eq. (1)]. Such simple relationships allow spectroscopists to analyze complex multichannel spectra and/or continuum processes (such as autoionization or recombination collisions) without explicit reference to the Coulomb functions. An early account of the present development has been published in Ref. [17].

The paper is organized as follows. In Sec. I we review the various Coulomb regular and irregular base pairs defined by Seaton [2] and the difficulties associated with their use. In Sec. III we define a class of energy-modified basis Coulomb functions designed to alleviate these difficulties. Their use is illustrated in Sec. IV with three examples, concerning the potassium atom, the nitric oxide radical, and the H_2 molecule. Section V provides a summary.

II. THEORY: BACKGROUND

A. False roots: An example

Figure 1 is a plot of n^*-l and $n-\mu$ versus n^* which illustrates how Eq. (1) works in practice. Bound levels occur whenever n^*-l (broken line) crosses one of the lines $n-\mu$ (full lines), corresponding to $n=1,2,\ldots$, thereby satisfying the bound-state condition given in Eq. (1). This plot is drawn for the example of the $P(l=1)$ series of neutral atomic potassium which illustrates the occurrence of spurious solutions and their relation to the energy dependence of the quantum defects. The p series of potassium is characterized by a quantum defect $\mu\approx 0.75$ with the first state appearing at $n^*=2.23$. It is not obvious from Eq. (1) alone why no p state may exist near $n^*=1.25$. (Note that whereas the convention adopted in Sec. II B below, in accordance with the prescription given in Ref. [12], has made us replace negative values of n^*-l with $l-n^*$, this is not done in Fig. 1 so as to more clearly show the behavior n^*-l and $n-\mu$ at low energy.) As may be seen from the figure, extrapolation of μ from $n^*\geq 3$ to lower values (dotted line) would indeed yield a spurious solution near $n^*=1.22$. However, as the figure also illustrates (based on a calculation which will be discussed in Sec. IV A below), the quantum defect in reality exhibits an energy dependence for $n^*<2$ in such a way that the false solution disappears. The two curves coincide for $n^*=1, n-\mu=0$: this point represents a trivial solution whose associated radial Rydberg wave function is zero everywhere.

In the remainder of this paper we denote the Coulomb effective principal quantum number $n^*=(-\epsilon)^{-1/2}$ by ν in accordance with most of the modern quantum-defect literature. We shall use Rydberg energy units except when indicated otherwise. For simplicity we will also assume that the charge of the ion core is $Z=1$. We shall further adopt Seaton's [2] notation for the various Coulomb base pairs, which differs from that used, e.g., by Fano [18] or Greene [9]. Table I of Ref. [2] provides the corresponding conversion table.

B. Phase-amplitude formulation

Given a base pair of radial functions $f_l(\epsilon,r)$ and $g_l(\epsilon,r)$, regular and irregular at the origin, $r=0$, which are solutions of the radial Schrödinger equation,

$$\left[\frac{\partial^2}{\partial r^2}+k_l^2(r)\right]\psi_l(r)=0,$$

$$k_l^2(r)=\epsilon-V_l(r)\equiv\epsilon+\frac{2}{r}-\frac{l(l+1)}{r^2}, \tag{5}$$

and which are linearly independent, we can construct an infinity of alternative base pairs, $(\tilde{f},\tilde{g})$, by appropriate superposition of the original functions. The most general transformation that ensures the regularity of $\tilde{f}$ and the irregularity of $\tilde{g}$ at the origin can be written in the form,

$$\begin{pmatrix}\tilde{f}_l\\ \tilde{g}_l\end{pmatrix}=\begin{pmatrix}A_l^{1/2} & 0\\ A_l^{-1/2}\tan\lambda_l & A_l^{-1/2}\end{pmatrix}\begin{pmatrix}f_l\\ g_l\end{pmatrix}, \tag{6}$$

where A_l and λ_l are free parameters. This transformation preserves the value of the Wronskian, i.e., $W(\tilde{f}_l,\tilde{g}_l)=W(f_l,g_l)$. Throughout this paper all base pairs are normalized so that their Wronskians are π^{-1} for negative as well as positive energies ϵ. For positive energies this implies energy normalization in Rydberg units. We follow Gorczyca and Badnell [12] and take the regular functions, f_l or $\tilde{f}_l$, to be real and positive near $r=0$, which implies that $A^{1/2}=+|A|^{1/2}$. The coefficients $A_l=A_l(\epsilon)$ and $\tan\lambda_l=\tan\lambda_l(\epsilon)$ in Eq. (6) are independent of r but can be functions of the channel energy ϵ. Indeed, it is this dependence that is the focus of the present work. Note that for convenience from here on we drop the partial-wave subscript l unless it is specifically needed.

We can generalize the concept of accumulated phase to the transformed functions of Eq. (6) by first writing the base pair in equivalent phase-amplitude form [15],

$$f(\epsilon,r)=+\sqrt{\frac{1}{\pi}}\alpha(\epsilon,r)\sin\phi(\epsilon,r),$$

$$g(\epsilon,r)=-\sqrt{\frac{1}{\pi}}\alpha(\epsilon,r)\cos\phi(\epsilon,r). \tag{7}$$

The transformed phase and amplitude functions then become

$$\tan\tilde{\phi}=\frac{A\tan\phi}{1-\tan\phi\tan\lambda}, \tag{8}$$

TABLE I. Seaton's base pairs for $\epsilon<0$. The table gives for each base pair the functions A and $\tan\lambda$ which relate it to f and g by means of Eq. (6). $\tan\tilde{\beta}$ is the accumulated phase parameter to be used in bound-state boundary conditions such as Eq. (11). $\nu=(-\epsilon)^{-1/2}$ is the effective principal quantum number (also denoted n^*), and l is the orbital angular momentum quantum number.

	A	$\tan\lambda$	$\tan\tilde{\beta}$
f,g	1	0	$\tan\beta=\frac{\tan\pi(\nu-l)}{\mathcal{A}(\epsilon,l)+\mathcal{G}(\epsilon,l)\tan\pi(\nu-l)}$
f,h	1	$\mathcal{G}(\epsilon,l)$	$\frac{\tan\pi(\nu-l)}{\mathcal{A}(\epsilon,l)}$
s,c	$\mathcal{A}(\epsilon,l)$	$\mathcal{G}(\epsilon,l)$	$\tan\pi(\nu-l)$

$$\tilde{\alpha}=\alpha A^{-1/2}\cos\phi[1+\tan\phi^2(A^2+\tan^2\lambda)]^{1/2}. \tag{9}$$

In the Milne phase-amplitude formulation [14] the accumulated phase parameter for $\epsilon<0$ (analogous to the quantity $\pi(\nu-l)$ mentioned above) is given by $\beta(\epsilon)=\lim_{r\to\infty}\phi(\epsilon,r)$. We can therefore use Eq. (8) with the limiting values as $r\to\infty$ and immediately obtain the equation for the effective accumulated phase $\tilde{\beta}$, i.e., the accumulated phase appropriate for the transformed functions of Eq. (6) as

$$\tan\tilde{\beta}=\frac{A\tan\beta}{1-\tan\beta\tan\lambda}. \tag{10}$$

C. Seaton's Coulomb base pairs

Seaton [2] used three different Coulomb base pairs which he denoted as (f,g) ("energy-independent normalization"), (f,h) ("Ham functions"), and (s,c) ("energy-normalized"), respectively. The functions (f,g) are analytic in energy and are energy independent near $r=0$. In order to have $W(f,g)=\pi^{-1}$ we normalize them by setting $\lim_{r\to0}(r^{-l-1}f)=[(2l+1)\pi]^{-1/2}$ and $\lim_{r\to0}(r^l g)=-[(2l+1)\pi]^{-1/2}$, respectively. (This differs from Seaton by an additional factor of $2^{-1/2}$.) Ham's functions (f,h) are "nearly analytic" since for most applications in QDT h may be treated as though it were an analytic function of ϵ [2]. The pairs (f,h) and (s,c) are related to (f,g) according to Eq. (6) with specific choices for the coefficients A and $\tan\lambda$. These are listed in Table I along with the phase parameters $\tilde{\beta}(\epsilon)$ from Eq. (10). The functions $\mathcal{A}(\epsilon,l)$ and $\mathcal{G}(\epsilon,l)$ which occur in the transformations are defined by Seaton ([2] Sec. 2.5), and they are displayed here in Fig. 2 as functions of the effective principal quantum number $\nu=(-\epsilon)^{-1/2}$ for $l=0-3$.

Note that the quantity $\mathcal{A}(\nu,l)$ is defined negative in Ref. [2] for certain ranges corresponding to $\nu\leq l$ [cf. Eq. (A4)]. We follow here again Ref. [12] by setting $\mathcal{A}^{1/2}=+|\mathcal{A}|^{1/2}$. This choice is equivalent to the application of an additional transformation of type Eq. (6) whenever $\mathcal{A}(\nu,l)$ is negative, with $A^{1/2}=-i$ and $\tan\lambda=0$ in this instance. From Eq. (10) it follows that the accumulated phase parameter $\tilde{\beta}$ then must also be replaced by its negative when $\mathcal{A}(\nu,l)$ is negative [12]. As shown by Table I, this convention concerns only the base pair (s,c). Further, we see from Eq. (4) that in a one-channel situation the quantum defect also changes sign because the factor f/g changes sign. The result is that Eq. (1) or Eq. (11) (below) remain valid without change. Therefore the change in sign of $\tilde{\beta}$ associated with the convention $\mathcal{A}^{1/2}=+|\mathcal{A}|^{1/2}$ when $\mathcal{A}$ is negative, is required only in multichannel problems and only when the (s,c) basis pair is used.

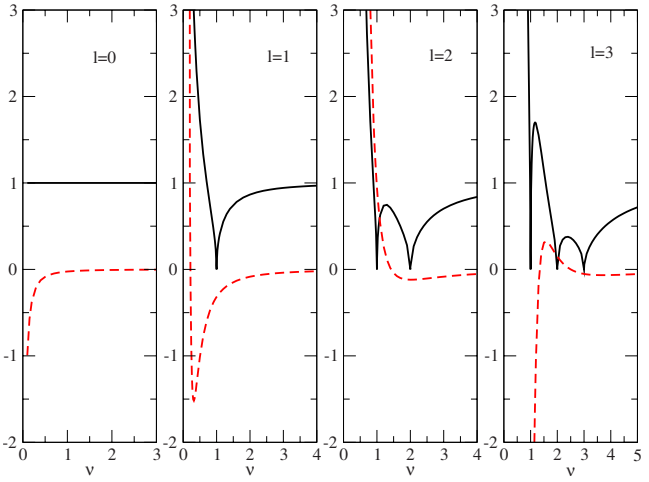

FIG. 2. (Color online). Functions $|\mathcal{A}(\epsilon,l)|^{1/2}$ (full lines) and $\mathcal{G}(\epsilon,l)$ (broken lines) for $l=0-3$, plotted versus the effective principal quantum number $\nu=(-\epsilon)^{-1/2}$. See Seaton ([2], Sec. 2.5) for the definitions of $\mathcal{A}$ and $\mathcal{G}$.

D. Problems with Seaton's base pairs

There are several problems arising when any of the base pairs listed in Table I are used for energies far below threshold. In a one-channel situation the quantization condition for bound states in the framework of quantum-defect theory reads as

$$\tan\beta(\epsilon)+\tan\pi\mu(\epsilon)=0, \tag{11}$$

or equivalently, generalizing Eq. (1),

$$\frac{\beta(\epsilon)}{\pi}+\mu(\epsilon)=n, n=1,2,\ldots, \tag{12}$$

where $\mu(\epsilon)$ is the quantum defect, which embodies the effect of interactions other than the Coulomb potential. That is, $\mu(\epsilon)$ accounts for interactions experienced by the scattering particle inside or near the core such as penetration effects and the effects of medium-range fields. As has already been mentioned in Sec. I, Eq. (12) is most useful in practical applications when (i) the quantum defect μ is constant as function of the energy ϵ or nearly so and when (ii) the accumulated phase parameter is a smooth function of energy which can be readily interpolated and extrapolated. Fulfillment of condition (i) depends on the interactions inside the core in the first place, but it also depends on the energy dependence of the base pair at the edge $r=r_c$ of the core, as mentioned earlier on and as one can see from Eq. (4). Independently of the logarithmic derivative of the inner function, ψ'/ψ (which itself might vary noticeably with energy, e.g., in the case of a shape resonance), a strong energy dependence of the base pair and the radial derivatives will invariably cause the quan-

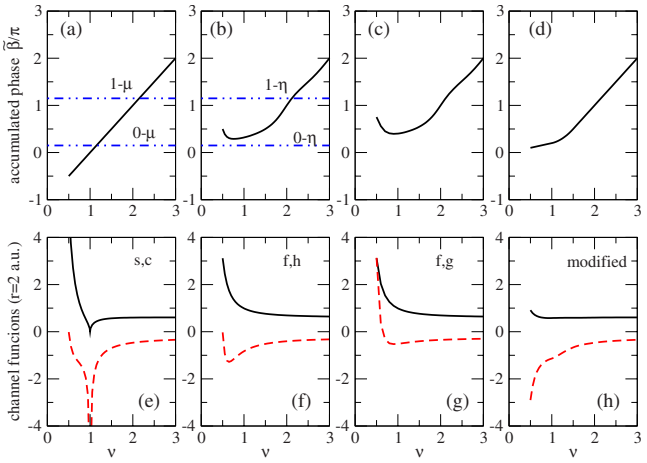

FIG. 3. (Color online) p wave: Upper panels (a)–(d): effective accumulated phase parameters $\tilde{\beta}/\pi$ plotted as functions of the effective principal quantum number $\nu \equiv n^*$ for different Coulomb base pairs. (a): (s,c), (b): (f,h), (c): (f,g), and (d): energy-modified base-pair (choice A with $a_1=0.34$, $b_1=0.2$, and $\delta_1=0.1$). See the text for more explanation. Lower panels (e)–(h): corresponding regular (full line) and irregular (broken line) function values for $r=2$.

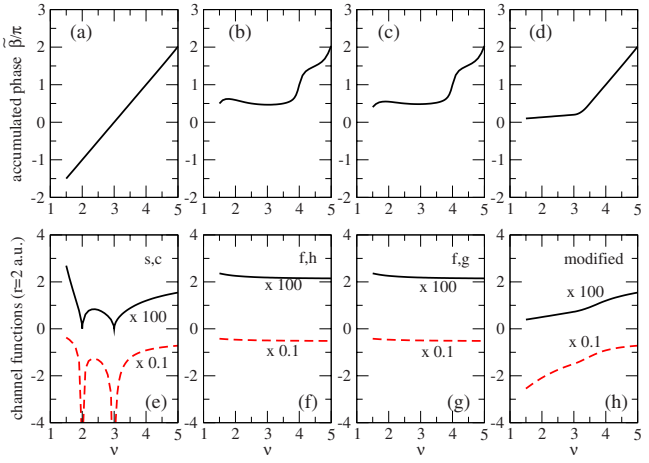

FIG. 4. (Color online) f wave: Upper panels (a)–(d): effective accumulated phase parameters $\tilde{\beta}/\pi$ plotted as functions of the effective principal quantum number $\nu \equiv n^*$ for different Coulomb base pairs. (a): (s,c), (b): (f,h), (c): (f,g), and (d): the energy-modified base-pair introduced here (choice A for the particular choice of parameters $a_3=0.13$, $b_3=0.2$, and $\delta_3=0.1$). Lower panels (e)–(h): corresponding regular (full line) and irregular (broken line) function values for $r=2$.

tum defect to exhibit a strong and (usually) undesirable energy dependence as well.

Figures 3 show that none of the three base pairs (f,g), (f,h), and (s,c) quite satisfy these requirements. The figure displays the effective accumulated phase parameter [Eq. (10) and implied in the last column of Table I] corresponding to each base pair for $l=1$ as function of the effective principal quantum number $\nu=(-\epsilon)^{-1/2}$. The plots further display the energy dependence of the $l=1$ base pairs for a particular r-radius, namely, $r=2$ a.u., which may be viewed as typical for the size of a small atomic or molecular core. Inspection of these figures shows that the pair (s,c) provides the most attractive option in terms of the energy dependence of the phase parameter β which in this case is simply the straight line $\pi(\nu-l)$ seen in Fig. 3(a). However, Fig. 3 also shows that below $\nu=2$, corresponding to the lowest physical hydrogen atom p-wave state, the corresponding Coulomb base pair, (s,c), acquires a strong energy dependence with s vanishing and c being infinite at $\nu=1$. As a consequence, the quantum defect will have a strong energy dependence in a realistic situation for any system in this region (cf. the example discussed in Sec. II A). Conversely, if in a model calculation the quantum defect is taken as a constant or nearly so or if it is simply extrapolated from higher energies where it is constant, unphysical solutions (e.g., $1p$, $1d$, $2d$, etc.) will occur for $\nu<l+1$ in the region where the channel is strongly closed. For instance, a quantum defect $\mu=-0.15$ [represented in Fig. 3(a) by a dot-dashed horizontal line corresponding to $-\mu$) will cross the curve representing β/π at $\nu=1.15$ and thus, according to Eq. (12), predict a $1p$ energy level at this ν value.

Further inspection of Fig. 3 indicates that the base pairs (f,g) and (f,h) are much less energy dependent at low energy than (s,c), and it is known that thereby many (although not always all) unphysical solutions can be avoided. Indeed it may be seen in Fig. 3(b) that the horizontal line representing the same quantum-defect value will not cross the accumulated phase curve corresponding to the (f,h) pair (η defect), and therefore no unphysical solution occurs near $\nu=1.15$ when a constant quantum defect is used. However, it is also apparent from the figures that a *strongly negative* quantum defect might still yield a false root. Further, it may be appreciated from Figs. 3(b) and 3(c) that the phase parameters associated with the pairs (f,h) and (f,g) have more complicated energy dependences for $\nu<l+1$ and also include undesirable undulations for $\nu>l+1$. In other words, the relationship between the accumulated phase and the effective principal quantum number no longer is simply linear, and thus a straightforward use of the Rydberg equation is no longer possible. Figure 4 is analogous to Fig. 3 and displays data for $l=3$. It can be seen that the problems just discussed not only persist at higher l but are in fact exacerbated.

III. ALTERNATIVE ENERGY-MODIFIED BASE PAIRS

A. Method

We now introduce a class of "energy-modified" base pairs which, while largely avoiding the problems just discussed, combine as best as possible the advantages of the base pairs listed in Table I. We start out with the function pair (f,g) which is analytic for all energies and energy independent near the origin $(f\sim[(2l+1)\pi]^{-1/2}r^{l+1}$ and $g\sim[(2l+1)\pi]^{-1/2}r^{-l})$. The functions f and g can be computed either using a series expansion as described by Seaton [19] or by direct numerical integration based on Milne's phase-amplitude formalism, see, e.g., Ref. [16]. According to Eq. (6) at every energy there are two free parameters at our disposal. We proceed by dividing the bound energy domain into three regions, the weakly closed region corresponding to ν

$\geq l+1-\delta_l$ (where $0 \leq \delta_l \leq 0.5$ is a small parameter which is introduced for convenience and will be specified later) and the strongly closed region corresponding to $\nu \leq l$. The region between those two zones we call the "transition region." These regions are analogous to Greene's [9] regions II, IV, and III, respectively.

Our approach consists of replacing one of the two free parameters of Eq. (6), $\tan \lambda_l$, by another, namely, the accumulated phase $\tilde{\beta}_l$. A_l and $\tilde{\beta}_l$ will then be conveniently parametrized, and $\tan \lambda_l$ will be evaluated as a function of them by means of the relation

$$\tan \lambda_l = \frac{1}{\tan \beta_l^{(fg)}} - \frac{A_l}{\tan \tilde{\beta}_l}, \tag{13}$$

which follows from Eq. (8). In this expression $\beta_l^{(fg)}$ is the effective accumulated phase parameter for the (f,g) base pair as given in Table I and which is illustrated in Figs. 3(c) and 4(c). $\tan \tilde{\beta}_l$ and A_l are the energy-modified phase and amplitude parameters which remain to be specified for each of the three regions. To summarize, our strategy is to *predefine* the accumulated phase parameter $\tilde{\beta}_l$ and the amplitude parameter A_l and their energy dependences in the weakly closed, strongly closed, and in the "transition" regions in a manner that will be easy to use in practice and which makes sense physically. We require further that the different regions must be connected smoothly. These choices are presented in Secs. III B–III D. We stress that our choices are, strictly speaking, arbitrary although we argue that they are physically reasonable. The infinite number of base pairs represented by Eq. (6) are indeed strictly equivalent. The present choices result from the experience acquired through numerous applications to real examples. They are justified by the success of the method in practice, but it is clear that different choices are also possible.

B. Weakly closed region

In the weakly closed region we choose the energy-modified base pair to be identical to Seaton's base pair (s,c). We therefore set

$$\tilde{\beta} = \beta = \pi(\nu - l) \quad \text{for} \quad \nu \geq l + 1 - \delta_l, \tag{14}$$

which implies that

$$A_l = \mathcal{A}(\epsilon, l),$$

$$\tan \lambda_l = \mathcal{G}(\epsilon, l) \quad \text{for} \quad \nu \geq l + 1 - \delta_l \tag{15}$$

in accordance with Eq. (6) and Table I. In Sec III D these weakly closed results will be smoothly connected to strongly closed ones. To do this the derivatives with respect to ν of $\tilde{\beta}$ and A_l at $\nu = l+1-\delta_l$ are needed. These are

$$\tilde{\beta}'(\nu = l + 1 - \delta_l) = \pi,$$

$$A_l'(\nu + 1 - \delta_l) = \mathcal{A}_l'(\nu + 1 - \delta_l, l), \tag{16}$$

where primes refer to derivatives with respect to ν.

C. Strongly closed region

In the strongly closed region corresponding to $\nu \leq l$, $k^2(r)$ in Eq. (5) is negative for all r, i.e., $k(r) = i\kappa(r)$ with κ real, so that asymptotically, as $\epsilon \to -\infty$, one has $\kappa(r) \sim \nu^{-1}$. The normalization of the Coulomb base pair and the related accumulated phase parameter $\tilde{\beta}(\epsilon)$ in this limit is arbitrary and has to be chosen on the basis of physical considerations. In Ref. [16] three different choices have been discussed in the context of the Milne phase-amplitude approach designed for QDT for arbitrary potentials (Greene *et al.* [15]).

(i) Energy normalization, with basis functions of the form $\kappa^{-1/2} \sinh[\kappa r]$ and $-\kappa^{-1/2} \cosh[\kappa r]$. This choice yields $\beta(\nu \to 0) = \pi/2$ (in analogy with the WKB result for classically forbidden regions) and was adopted in Ref. [13]. On the basis of the arguments put forward in Ref. [9], as explained in Sec. I, above, we do not make this choice here.

(ii) Choice A: "energy-independent normalization," using a base pair of the form $\kappa^{-1} \sinh[\kappa r]$ and $-\cosh[\kappa r]$ as suggested previously in Ref. [15]. This choice implies $\tilde{\beta}(\nu \to 0) \sim q\nu$ (where q is a real scaling factor) in agreement with our requirement that the accumulated phase should approach zero at asymptotically low energies. We refer to this choice as "choice A."

(iii) Choice B: "exponential normalization," based on a pair of the form $e^{-q\kappa} \sinh[\kappa r]$ and $-e^{+q\kappa} \cosh[\kappa r]$. These forms imply [16] that phase accumulation in the forbidden region occurs only to the extent that wave functions deviate from purely exponential form $e^{\pm \kappa r}$. This choice yields $\tilde{\beta}(\nu \to 0) \sim e^{-q/\nu}$ so that the phase also tends to zero with this definition. This choice has been adopted in the numerical applications based on Ref. [16], and we refer to it as "choice B."

We now use limiting cases A and B to set up two different parameterizations of the accumulated phase, $\tilde{\beta}$, for the strongly closed region, $\nu \leq l$. Since $\tilde{\beta}$ is a free parameter we use the simple expedient of extending the limiting functional behavior of choices A and B from $\nu \to 0$ all the way up to $\nu = l$. This upper limit is still a deeply closed energy as it corresponds to the nominal $0s$, $1p$, etc. states. With $\tilde{\beta}/\pi$ set to 0 at $\nu = 0$ and to 1 at $\nu = l+1$ we chose the parameter b_l between these two values and set

$$\tilde{\beta}_l(\nu = l) = \pi b_l. \tag{17}$$

[More precisely, b_l should be chosen so that as $\tilde{\beta}$ increases from $\nu = 0$ to l it does not "overshoot" its lowest value in the weakly closed region which, from Eq. (14) is seen to be $1 - \delta_l$]. For $\tilde{\beta}$ to assume the desired value at $\nu = l$ the parameter q must be chosen as b_l for choice A and $-l \ln b_l$ for choice B. Thus, in the strongly closed region, β_l and its derivative with respect to ν (needed below, for connection to the transition region) are

$$\tilde{\beta}_l = \pi \frac{b_l}{l} \nu,$$

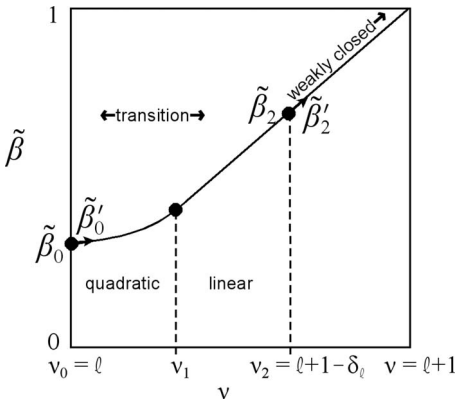

FIG. 5. Quadratic plus linear bridging function connecting the points $\nu=l$ and $\nu=l+1$ (strongly closed and weakly closed regions, cf. the text).

$$\frac{\partial\tilde{\beta}_l}{\partial\nu}=\pi\frac{b_l}{l},\quad \nu\le l(\text{choice A}),$$

$$\tilde{\beta}_l=\pi e^{l\ln b_l/\nu},$$

$$\frac{\partial\tilde{\beta}_l}{\partial\nu}=-\pi\frac{l\ln b_l}{\nu^2}e^{l\ln b_l/\nu},\quad \nu\le l(\text{choice B}). \tag{18}$$

The second parameter in specifying the transformed basis pair of Eq. (6) is the amplitude, A_l. We chose

$$A_l=\frac{a_l}{l^2}\nu^2,\quad \nu\le l. \tag{19}$$

This choice takes A_l to zero as $\nu\to 0$, and Eq. (6) then implies the same for $\tilde{f}$. Applying Eq. (3) to the transformed base pair leads to a related quantum defect, which we denote $\tilde{\mu}$. Since the choice of A_l in Eq. (19) implies $\tilde{f}(\nu\to 0)=0$, Eq. (4) tells us that we now have $\tilde{\mu}(\nu\to 0)=0$, as desired. We note, finally, that for a given l, the only free parameters are the dimensionless quantities b_l [Eq. (18)] and a_l [Eq. (19)].

D. Transition region

As shown for $\tilde{\beta}$ in Fig. 5, we cover the gap between the strongly closed ($\nu\le l$) and weakly closed ($\nu>l+1-\delta_l$) regions by using bridging functions for $\tilde{\beta}(\nu)$ and $A_l(\nu)$ in this transition region. In the lower end of this transition region we use a quadratic function, while in the upper end of the transition region a linear function is used. That is, each of $\tilde{\beta}_l$ and A_l are modeled by the functions

$$\begin{aligned} y(\nu)&=c_0+c_1\nu+c_2\nu^2, \quad \nu_0\le\nu\le\nu_1,\\ y(\nu)&=d_0+d_1\nu, \qquad\qquad \nu_1\le\nu\le\nu_2. \end{aligned} \tag{20}$$

The coefficients c_i and d_i are chosen so that $\tilde{\beta}_l(\nu)$ and $A_l(\nu)$ and their first derivatives with respect to ν are continuous at each of the three connecting points (shown by the solid circles in Fig. 5). For each of $\tilde{\beta}_l(\nu)$ and $A_l(\nu)$ we therefore have two conditions at each of three points. As detailed in the Appendix these six conditions fix the values of the c_i and d_i, along with the value of the transition matching point ν_1.

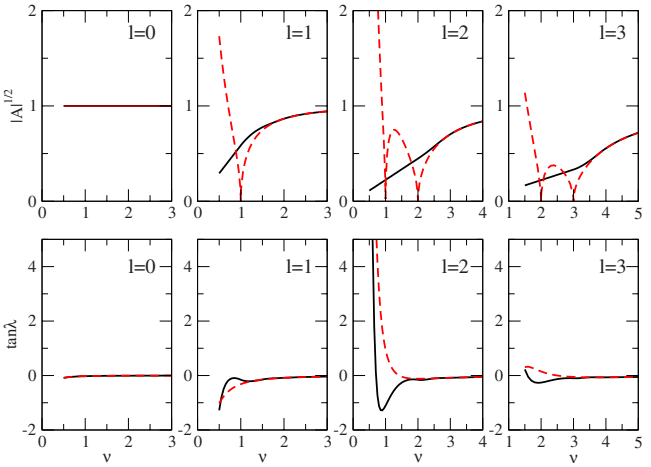

FIG. 6. (Color online). Amplitude ($|A_l|^{1/2}$, top) and phase (tan λ_l, bottom) parameters as functions of the effective principal quantum number ν for a Coulomb field with $l=0-3$ (from left to right). Full line: energy modified. Dashed line: Seaton's pair (s,c).

Once a_l, b_l, and δ_l have been specified, $\tilde{\beta}_l$ and A_l are defined for all positive values of ν and hence for all negative energies ϵ. Typical choices are $a_l=b_l=0.2$ and $\delta_l=0.1$. Note that the minimum of the Coulomb potential for $l\ge 0$ corresponds to $\nu_{\min}=\sqrt{l(l+1)}$, which in turn corresponds to $\delta_l=\frac{1}{2}+[l+\frac{1}{2}-\sqrt{l(l+1)}]\approx\frac{1}{2}$. A choice of δ_l in the interval $0\le\delta_l\le\frac{1}{2}$ therefore places the ν_1 transition matching point above the potential minimum, yet lower than the lowest hydrogenic level $n=l+1$.

Figure 6 illustrates the energy-modified parameters A_l and tan λ_l obtained with choice A as functions of ν for $l=0-3$ and compares them with the corresponding parameters associated with the energy-normalized (s,c) Coulomb pair. In Sec. IV we discuss examples treated with energy-modified Coulomb functions resulting from choice A which is particularly attractive because of the very simple energy dependence of the associated accumulated phase parameter $\tilde{\beta}$.

IV. APPLICATIONS

A. ^2P *np* series of *K* I

Parsons and Weisskopf [20] showed that the observed positions of the bound states of all alkali-metal atoms can be reproduced quite accurately when the atomic ion core is represented by a hard sphere with a suitably chosen radius r_c. Following these authors we take the radial potential (in Rydberg units) as

$$V(r)=\frac{l(l+1)}{r^2}-\frac{2}{r}+V_c,\quad r<r_c,$$

$$V(r)=\frac{l(l+1)}{r^2}-\frac{2}{r},\quad r>r_c, \tag{21}$$

where for potassium ($l=1$) we use $V_c=100$ Ry and $r_c=1.63$ a.u. to simulate the hard sphere [20]. The radial func-

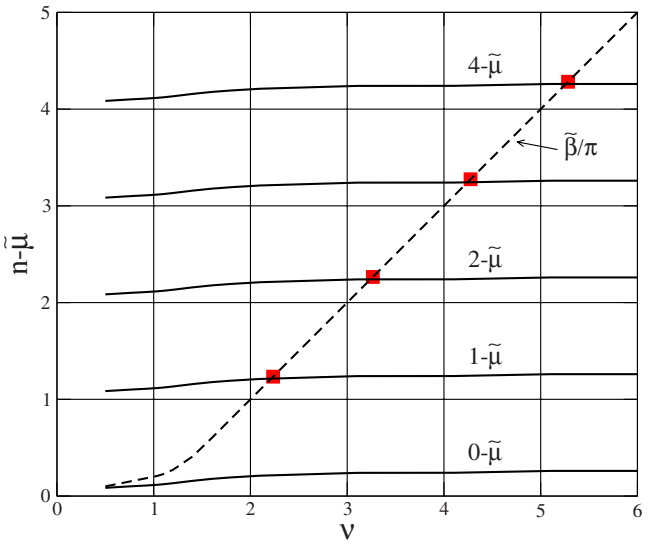

FIG. 7. (Color online) ^2P *np* series in potassium: same as Fig. 1 but with $\tilde{\mu}$ calculated using the energy-modified base pair ($a_1=b_1=0.2, \delta_1=0.1$).

tion $\psi(r)$, regular at the origin, is evaluated by numerical Numerov propagation for arbitrary energy using the potential of Eq. (21). Equation (4) then yields the quantum defect μ, with f and g taken as any pair of Coulomb channel functions corresponding to the same energy. Figures 1 and 7 are plots of the accumulated phase parameter (broken line) and the quantity $n-\mu$ (full lines, n integer) versus the effective principal number, evaluated with the Coulomb pairs (s,c) (Fig. 1) and the energy-modified pair $(\tilde{f},\tilde{g})$ (Fig. 7). The two calculations yield identical bound levels (crossings of the broken and full lines) which compare quite favorably with the experimental values (squares). However, we see that the quantum defect corresponding to the energy-modified Coulomb base pair exhibits a weaker energy dependence in the strongly closed region than the quantum defect obtained with Seaton's standard Coulomb pair. The occurrence of the unphysical state near $\nu\approx 1.25$ is avoided in both calculations, but when the standard base pair (s,c) is used this happens at the expense of the strong energy dependence of μ in the strongly closed region visible in Fig. 1. This dependence cannot be anticipated from higher-energy behavior and is only evident with a detailed calculation in the core region.

B. Lowest $^2\Sigma^+$ Rydberg states of NO

The Rydberg series of nitric oxide converging to the ground state of the ion NO^+ exhibit the effects of strong l mixing that varies substantially with the nominal l value of the various series and also with effective principal quantum number along some of the series [21,22]. The strongest effects occur near equilibrium in the "*s*" and "*d*" $^2\Sigma^+$ series which, for $\nu\geq 3$, are 60–40 % and 40–60 % mixtures, respectively, of the pure $l=0$ and 2 partial waves. By contrast, the lowest member of the *s* series, $3s\sigma$, has no $2d$ counterpart to interact with and therefore exhibits nearly—but not quite—pure *s* character as has been deduced both on experimental grounds [21] as well as from quantum-chemical calculations [23,24]. As a result the l character of the *s* Rydberg series varies strongly with principal quantum number for low ν.

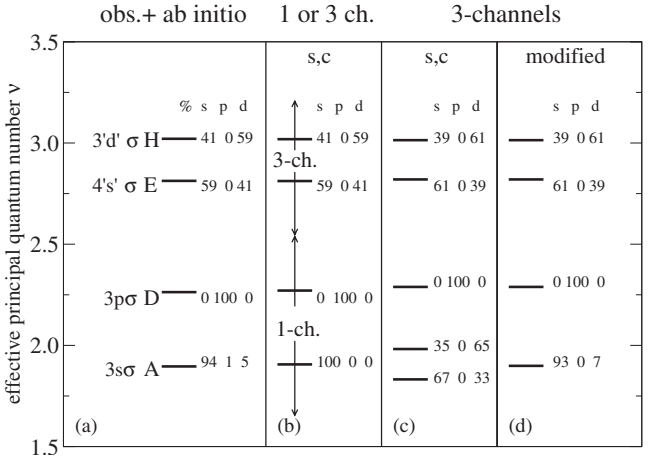

FIG. 8. Effective principal quantum numbers ν of low-lying $^2\Sigma^+$ Rydberg states of NO. Observed (see Ref. [21]) (a) and MQDT calculated (b)–(d) values are indicated by horizontal bars. For each state the fractional decomposition into l partial waves is given [from Refs. [21], [23], and [24] for panel (a)]. Quantum defects for all MQDT calculations are based on the artificial well *ab initio* calculations of Ref. [29]. A penetration contribution $\Delta\nu=-0.056$ [29] has been added uniformly to all *ab initio* calculated level positions in panels (b)–(d). Panel (b) using a 3×3 quantum-defect matrix ($l=0-2$) for $\nu\geq 2.5$ and a 1×1 matrix ($l=0$ or 1 for $\nu\leq 2.5$ (corresponding to the full lines and circles in Fig. 9). [(c) and (d)] Using a 3×3 matrix throughout (corresponding to the broken lines in Fig. 9): (c) with Seaton's base pair (s,c). (d) with the energy-modified Coulomb base pair. (cf. the text for details).

The quantum-chemical calculations show that the $3s\sigma A^2\Sigma^+$ state contains a *d*-type contribution of about 5% [see Fig. 8(a)]. This explains why in resonantly enhanced multiphoton ionization (REMPI) spectroscopy involving the *A* state as intermediate state the *f* Rydberg series are excited with substantial intensity (see e.g., Refs. [25,26] and references therein). Recent direct *ab initio* *R*-matrix type calculations of quantum defects combined with MQDT evaluations of bound-state energies [27–29] account quite accurately for the strong *s*-*d* mixing occurring for $\nu\geq 3$ [$(n+1)s\sigma$ and $nd\sigma$ pairs of states], but they fail to reproduce the small *d* contribution present for $\nu\approx 2$ ($3s\sigma A$ state). The reason is that below $\nu\approx 3$ the strongly closed $d\sigma$ Rydberg channel was not explicitly included as an asymptotic channel in either Ref. [27] or Ref. [29], with the result that the lowest *s* Rydberg state was calculated with 100% *s* character [Fig. 8(b)]. This is illustrated by Fig. 9 where the quantum-defect matrix elements for NO $^2\Sigma^+$ calculated with the approach of Ref. [29] are plotted versus the Rydberg energy ϵ. Below $\epsilon\approx -0.1$, only the *s* and *p* channels subsist because the strongly closed channels were excluded. Notice that the slope of the line representing the $\mu_{ss\sigma}$ matrix element (full line) exhibits a discontinuity between the two lowest calculated points, that is, somewhere roughly between $\nu=2$ ($\epsilon=-0.25$) and $\nu=3$ ($\epsilon=-0.11$). (To a lesser extent this is seen to happen also for the $\mu_{pp\sigma}$ matrix element.) Above this energy all the matrix

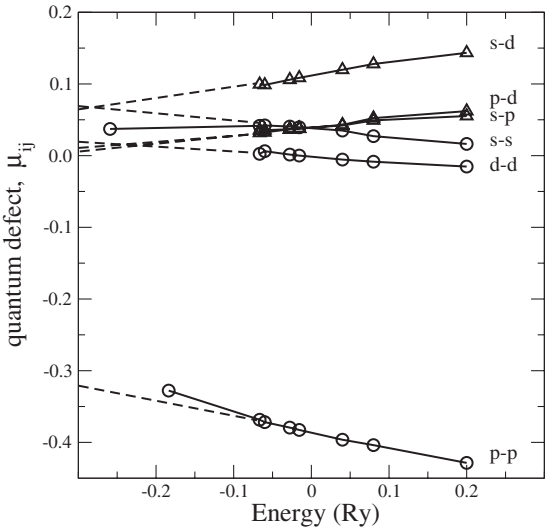

FIG. 9. Quantum-defect matrix elements $\mu_{l,l'}$ $(l,l'=0-2)$ for NO, $^2\Sigma^+$ symmetry, as functions of the energy. Circles (diagonal) and triangles (off-diagonal) connected by full lines: *ab initio* values evaluated with the approach of Ref. [29]. Broken lines: linear extrapolation from $\epsilon \geq -0.08$ toward lower energy.

elements exhibit a more or less linear and rather weak energy dependence. Linear extrapolation toward lower energy yields the values represented by the broken lines in Fig. 9. Of course it cannot be taken for granted *a priori* that an *R*-matrix calculation at these low energies carried out by retaining the strongly closed channels would indeed yield the quantum-defect values predicted by this extrapolation. However, based on the potassium example discussed above, we may hope that an *R*-matrix calculation carried out with the energy-modified Coulomb base pairs would produce less energy dependence than, e.g., Seaton's base pair (s,c). Figure 8 graphically represents the results obtained in a MQDT calculation using the extrapolated quantum defects from Fig. 9 (i.e., not taking into account the change in slope seen for $\epsilon < -0.1$ Ry), combined with the pairs (s,c) for $l=0-2$ (panel c). Also shown are the results obtained when energy-modified Coulomb base pairs are used (panel d). If the pairs (s,c) are used, an unphysical state $2d$ is seen to occur, giving an unphysical strong *s*-*d* *l* mixing effect which pushes the lowest member of the *s* series to an incorrect position. If on the other hand energy-modified base pairs are used in the calculation, the unphysical solution disappears and the lowest *s* Rydberg state is obtained near its observed position. Moreover, Fig. 8(d) indicates that the weak *d* contribution to this state is obtained approximately correctly as well. This is a useful result because it opens the possibility of incorporating the *A* state in a full MQDT treatment of photoionization of NO proceeding through this state and thus to model, e.g., the recent time-resolved photoelectron imaging studies of the Suzuki *et al.* [30] in a full scattering theoretical framework.

C. $^1\Delta_g$ Rydberg channels of H_2

Molecular hydrogen H_2 exhibits numerous examples of Rydbergization [5,6], where states which clearly have Rydberg character for small values of the internuclear distance *R*, turn adiabatically into valence-type states as *R* gets larger and dissociation is approached. The best known example is furnished by the manifold of $^1\Sigma_g^+$ symmetry where the $(1\sigma_g)\epsilon s\sigma$ Rydberg channel built on the H_2^+ $(1\sigma_g)$ ground-state core gets increasingly mixed with the core-excited $(1\sigma_u)^2$ valence configuration as the vibrational excitation increases. Unlike the two preceding examples we present here a full treatment of the two electron problem including a variational *R*-matrix calculation combined with MQDT, and for the purpose of illustration we choose the channels of $^1\Delta_g$ symmetry.

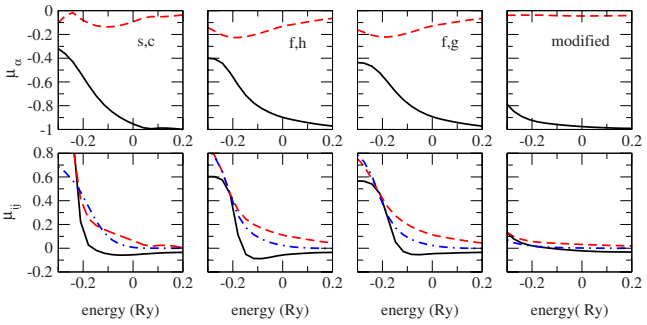

FIG. 10. (Color online) Quantum-defect matrices for H_2 $^1\Delta_g, R=3.4$ a.u. as functions of the energy [$\epsilon=0$ corresponds to the $(1\sigma_g)H_2^+$ ground state]. Upper row of panels: eigenquantum defects μ_α. Bottom row of panels: matrix μ_{ij} (full line: $i=1,j=1$, dashed line: $i=1,j=2$, and dot-dashed line: $i=2,j=2$). Columns, from left to right: matrices corresponding to the base pairs (s,c), (f,h), (f,g), and energy-modified, respectively (see the text for details).

A calculation on $^1\Delta_g$ Rydberg states of H_2 has been carried out for an internuclear distance $R=3.4$ a.u. using the variational *R*-matrix code of Refs. [4,31] implemented with spheroidal coordinates ξ,η,ϕ. In the asymptotic zone $\xi \geq \xi_0$ we explicitly included the channels with $^1\Delta_g$ symmetry corresponding to $\tilde{l} \leq 3$ and the ground and first excited state cores, viz. $1\tilde{s}\sigma_g\epsilon\tilde{d}\delta_g$ and $2\tilde{p}\sigma_u\epsilon\tilde{f}\delta_u$. The external channel functions $\epsilon\tilde{l}\lambda$ were evaluated in the effective "halfium" spheroidal framework, where the outer electron is described moving in the field of two charges $Z=\frac{1}{2}$ separated by *R*.

The quantum-defect matrix evaluated in the present example has dimension 2×2 and initially corresponds to spheroidal wave functions. In order to obtain matrices corresponding to spherical angular wave functions (spherical harmonics), the spheroidal variational eigensolutions were projected onto a sphere, centered on the molecular midpoint, and enclosing the spheroidal reaction volume $\xi=\xi_0$. An *R*-matrix-type matching procedure [10] carried out on this sphere then yielded the desired spherical reaction matrix elements K_{ij}, $(i,j=1$ and $2)$. This matching procedure was carried out successively with the channel functions (s,c), (f,h), (f,g), and the energy-modified pair $(\tilde{f},\tilde{g})$, respectively.

Figure 10 illustrates the results. It depicts, from left to right, the quantum defects as functions of the energy, calculated, respectively, with the energy-normalized base pairs, with Ham's functions, with the energy-independent pairs and with the energy-modified base pairs. As this is a multichan-

TABLE II. Effective principal quantum numbers ν of $^1\Delta_g$ Rydberg states of H_2 (R=3.4 a.u.).The table gives the clamped-nuclei ν values of bound states calculated by combining the variational R-matrix approach with MQDT, using different Coulomb base pairs as indicated. The states calculated with $\nu \approx 2$ are unphysical.

State	Exact[a]	s,c	f,h	f,g	Energy Modified	Exact-calc.
		2.007				
		2.057	2.062	2.066		
$J\ ^1\Delta_g$	3.042	3.034	3.035	3.035	3.034	+0.008
$S\ ^1\Delta_g$	4.041	4.038	4.038	4.037	4.038	+0.003
		5.038	5.039	5.039	5.038	
		6.038	6.039	6.039	6.039	

[a]From Wolniewicz [32] (interpolated).

nel problem, the quantum defects can be plotted in various ways. The top panels represent the eigenquantum defects

$$\mu_\alpha = \pi^{-1} \tan^{-1} \sum_{kk'} U^{-1}_{\alpha k} K_{kk'} U_{k'\alpha}, \tag{22}$$

where $K_{kk'}$ are the elements of the reaction matrix which is produced by the variational calculation and U is the matrix of its eigenvectors. The second row of panels of Fig. 10 presents the quantum-defect matrix elements $\boldsymbol{\mu}=\tan^{-1}\mathbf{K}$ (where the arctan is taken element by element). Remembering that quantum defects are defined mod 1 Fig. 10 demonstrates that the use of the energy-modified Coulomb functions leads to a striking reduction in the energy dependences. In particular, the elements μ_α and $\mu_{ii'}$ exhibit virtually no energy dependence down to quite low energies, whereas all three other types of base pairs produce a strong resonance centered at $\epsilon=-0.25$ resulting in an avoided crossing displayed by the eigenquantum defects.

We stress that the physical content of all the matrices represented in Fig. 10 is exactly the same. This is demonstrated by Table II where the effective principal quantum numbers calculated by MQDT with the set of matrices $\boldsymbol{\mu}$ displayed in Fig. 10 are listed. The table also lists the effective principal quantum number values derived from the best available quantum-chemical *ab initio* calculations of Wolniewicz [32] for the J and S states of H_2. The present R-matrix calculation combined with MQDT evaluation yields the lowest $^1\Delta_g$ state, J, for R=3.4 a.u. correctly to within 60 cm^{-1} and the second state, S, correctly to within 10 cm^{-1}. The fact that the R-matrix calculation combined with MQDT bound-state energies are lower than the quantum-chemical results is due to the fact that we have added a polarization correction in the external zone. Table II finally shows that the evaluations based on the Coulomb pairs (s,c), (f,h), and (f,g) produce false roots near ν=2 where no $2d\delta$ state can exist, while the calculation carried out with the energy-modified pairs does not produce such false roots. The occurrence of false roots in Table II is somewhat surprising since a full calculation inside the core as well as in the asymptotic zone has been carried out here so that no unphysical solutions are expected. What Table II reveals is that the energy step size (0.03 Ry) used in the variational R-matrix treatment has not been small enough for the MQDT code to cope correctly with the extreme energy dependences exhibited by the $\boldsymbol{\mu}$ matrix (Fig. 10). The need for smooth quantum-defect matrices is thereby once again demonstrated.

V. SUMMARY

The present development is intended to facilitate multichannel quantum-defect calculations on Rydberg states of atoms and molecules. It should remove some of the problems which arise when quantum-defect theory is applied to low-lying states. These are the strong and unexpected energy dependences of quantum defects at low energies and the ensuing appearance of unphysical states in the calculations (false roots) in this range. These problems are typically due to the fact that the Rydberg equation $\nu=(-\epsilon)^{-1/2}$ is used to relate the radial Rydberg accumulated phase $\beta(\epsilon)$ to the energy by setting $\beta(\epsilon)=\pi(\nu-l)$ even in strongly bound channels. However, although this may not be explicitly apparent in some applications, this relationship is synonymous with using Coulomb functions (Seaton's [2] functions s and c in particular) which for certain low energies vanish identically or diverge.

Our approach retains the simple relationship between radial phase and energy which makes the empirical multichannel quantum-defect theory so effective. However, this relationship now takes different forms depending on whether a particular channel is weakly closed, strongly closed, or transitional. The expressions for the corresponding accumulated phase parameters are given by Eqs. (14), (18), and (20) [together with Eq. (A1) and the appropriate parameters from Table III]. In particular these simple expressions should enable spectroscopists to carry out elaborate multichannel fitting procedures of complex Rydberg spectra without explicit reference to the Coulomb functions used—just as is the case when the familiar Rydberg relationship is used in MQDT applications. Detailed knowledge of the functions themselves will not be required except when quantum defects are calculated from first principles, e.g., in a R-matrix framework or when dipole transition moments are evaluated in the Coulomb approximation. The energy-modified Coulomb functions are expressed in terms of the well-documented function pair (f,g) (energy-independent normalization near the origin) [2] by the transformation [Eq. (6)], with values for A_l

TABLE III. Values to be used in Eqs. (A1)–(A3).

	y_0	y_0'	y_2	y_2'
		Choice A		
$\tilde{\beta}/\pi$	b_l	$\frac{b_l}{l}$	$1-\delta_l$	1
A_l	a_l	$2\frac{a_l}{l}$	$\mathcal{A}(\nu=1-\delta_l,l)$	$\mathcal{A}'(\nu=1-\delta_l,l)$
		Choice B		
$\tilde{\beta}/\pi$	b_l	$-\frac{b_l}{l}\ln b_l$	$1-\delta_l$	1
A_l	a_l	$2\frac{a_l}{l}$	$\mathcal{A}(\nu=1-\delta_l,l)$	$\mathcal{A}'(\nu=1-\delta_l)$

and $\tan\lambda_l$ defined in Sec. III for the different regions.

Finally, we note that an earlier version of the energy-modified Coulomb functions has already been used. The earlier version of the $\tilde{g}_l$ functions had no admixture of f_l, i.e., the transformation matrix in Eq. (6) was taken as diagonal so that $\lambda_l=0$, and $\tilde{\beta}_l$ was thereby implicitly defined through Eq. (13). Also, the transition region was taken as extending from $\nu=l$ to $\nu=l+1$ (rather than $l+1-\delta_l$) and the bridging function was taken as a single cubic spline. This earlier version was used with some success, for example, in the work reported in Refs. [17,33].

ACKNOWLEDGMENTS

R.G. has been suported in part by the French National Research Agency (project Corymol, ANR-05–NT05–2_41885). Ch.J. expresses his thanks to Dr. C. H. Greene (Boulder, Colorado) for stimulating discussions, and the Joint Institute for Laboratory Astrophysics (JILA) at Boulder for their hospitality during a stay during which part of the present paper was written. Ch.J. also benefited from support by the E. Miescher Foundation (Basel, Switzerland). Support by the Department of Chemistry and Applied Biosciences, ETH Zürich (Switzerland) is also gratefully acknowledged. S.C.R. acknowledges the ongoing support of the Natural Sciences and Engineering Research Council of Canada. H.O. acknowledges financial support from the Institut Français de Coopération (IFC) in Tunis. M.T. is grateful for partial support by the CNRS/DGRSRT French-Tunisian Cooperation Project (PICS).

APPENDIX: TRANSITION REGION BRIDGING FUNCTIONS

As discussed in Sec. III D and as shown for $\tilde{\beta}$ in Fig. 5, we bridge the gap between the weakly and strongly closed regions by use of a smoothly connected quadratic and linear functions [Eq. (20)]. This gap extends from $\nu_0=l$ to $\nu_2=l+1-\delta_l$ and, as also shown in Fig. 5, the quadratic bridging function is used from ν_0 to ν_1 and the linear one from ν_1 to ν_2. The transition matching point, ν_1, and the five expansion coefficients of Eq. (20) are chosen to ensure the continuity of the function being bridged [which we denote $y(\nu)$], and its first derivative with respect to ν [which we denote $y'(\nu)$] at the three points ν_0, ν_1, and ν_2. Straightforward algebra taking into account these six conditions yields the coefficients c_i and d_i in terms of the given values y_0, y_0', y_2, and y_2':

$$c_2=\frac{1}{4}\frac{(y_2'-y_0')^2}{[y_2'(\nu_2-\nu_0)-(y_2-y_0)]},$$

$$c_1=-2c_2\nu_0+y_0',$$

$$c_0=c_2\nu_0^2-y_0'\nu_0+y_0,$$

$$d_1=y_2',$$

$$d_0=y_2-y_2'\nu_2. \tag{A1}$$

The connection point ν_1 between the quadratic and linear forms of $y(\nu)$ is found to be

$$\nu_1=\nu_0+\frac{2[y_2'(\nu_2-\nu_0)-(y_2-y_0)]}{y_2'-y_0'}. \tag{A2}$$

In choosing a_l [Eq. (19)] and b_l (one of the relations [Eq. (18)]) it must be remembered to ensure that the transition matching point, ν_1, lies between ν_0 and ν_2. This means that the following conditions must be verified: if $y_2'-y_0'\geq 0$:

$$y_0+\frac{1}{2}y_0'(\nu_2-\nu_0)\leq y_2-\frac{1}{2}y_2'(\nu_2-\nu_0),$$

$$y_0\geq y_2-y_2'(\nu_2-\nu_0),$$

if $y_2'-y_0'\leq 0$:

$$y_0+\frac{1}{2}y_0'(\nu_2-\nu_0)\geq y_2-\frac{1}{2}y_2'(\nu_2-\nu_0),$$

$$y_0\leq y_2-y_2'(\nu_2-\nu_0). \tag{A3}$$

Table III gives the values for y_0, y_0', and y_2, y_2' to be used in Eqs. (A1)–(A3) for choices A and B. $\mathcal{A}(\nu,l)$ and its derivative can be taken from Eq. 2.57 of Seaton [2] and are

$$\mathcal{A}(\nu,l)=\left(1-\frac{1^2}{\nu^2}\right)\left(1-\frac{2^2}{\nu^2}\right)\cdots\left(1-\frac{l^2}{\nu^2}\right),$$

$$\mathcal{A}'(\nu,l)=\frac{2}{\nu^3}\mathcal{A}(\nu,l)\left[\frac{1^2}{1-\frac{1^2}{\nu^2}}+\frac{2^2}{1-\frac{2^2}{\nu^2}}+\cdots+\frac{l^2}{1-\frac{l^2}{\nu^2}}\right]. \tag{A4}$$

Using the values for choice A from Table III in Eq. (A3) immediately implies that

$$0\leq b_l\leq\frac{l}{2l+1}. \tag{A5}$$

[1] *Molecular Applications of Quantum Defect Theory*, edited by Ch. Jungen (The Institute of Physics, Bristol, 1996).
[2] M. J. Seaton, Rep. Prog. Phys. **46**, 167 (1983) reprinted in Ref. [1].
[3] S. C. Ross and Ch. Jungen, Phys. Rev. A **49**, 4364 (1994).
[4] S. Bezzaouia, M. Telmini, and Ch. Jungen, Phys. Rev. A **70**, 012713 (2004).
[5] R. S. Mulliken, Acc. Chem. Res. **9**, 7 (1976).
[6] R. S. Mulliken, Chem. Phys. Lett. **46**, 197 (1977).
[7] R. S. Mulliken, Phys. Rev. **32**, 186 (1928).
[8] M. Raoult, J. Chem. Phys. **87**, 4736 (1987). (cf. in particular Fig. 3 and the accompanying discussion).
[9] C. H. Greene, Phys. Rev. A **20**, 656 (1979).
[10] U. Fano and A. R. P. Rau, *Atomic Collisions and Spectra* (Academic, Orlando, 1986), Chap. 6.4.
[11] F. S. Ham, Solid State Phys. **1**, 127 (1955).
[12] T. W. Gorczyca and N. R. Badnell, J. Phys. B **33**, 2511 (2000).
[13] M. S. Child and M. Hiyama, J. Phys. B **40**, 1233 (2007).
[14] W. E. Milne, Phys. Rev. **35**, 863 (1930).
[15] C. H. Greene, A. R. P. Rau, and U. Fano, Phys. Rev. A **26**, 2441 (1982).
[16] Ch. Jungen and F. Texier, J. Phys. B **33**, 2495 (2000).
[17] S. C. Ross, Ch. Jungen, and A. Matzkin, Can. J. Phys. **79**, 561 (2001).
[18] U. Fano, Phys. Rev. A **2**, 353 (1970).
[19] M. J. Seaton, Comput. Phys. Commun. **25**, 87 (1982).
[20] R. G. Parsons and V. F. Weisskopf, Z. Phys. **202**, 492 (1967).
[21] Ch. Jungen, J. Chem. Phys. **53**, 4168 (1970).
[22] S. Fredin, D. Gauyacq, M. Horani, Ch. Jungen, G. Lefevre, and F. Masnou-Seeuws, Mol. Phys. **60**, 825 (1987).
[23] K. Kaufmann, C. Nager, and M. Jungen, Chem. Phys. **95**, 385 (1985).
[24] S. N. Dixit, D. L. Lynch, V. McKoy, and W. M. Huo, Phys. Rev. A **32**, 1267 (1985).
[25] W. Y. Cheung, W. A. Chupka, S. D. Colson, D. Gauyacq, P. Avouris, and J. J. Wynne, J. Phys. Chem. **90**, 1086 (1986).
[26] A. L. Goodgame, H. Dickinson, S. R. Mackenzie, and T. P. Softley, J. Chem. Phys. **116**, 4922 (2002).
[27] M. Hiyama and M. S. Child, J. Phys. B **35**, 1337 (2002).
[28] R. Guérout, M. Jungen, and Ch. Jungen, J. Phys. B **37**, 3043 (2004).
[29] R. Guérout, M. Jungen, and Ch. Jungen, J. Phys. B **37**, 3057 (2004).
[30] M. Tsubouchi and T. Suzuki, J. Chem. Phys. **121**, 8846 (2004).
[31] M. Telmini and Ch. Jungen, Phys. Rev. A **68**, 062704 (2003).
[32] L. Wolniewicz, J. Mol. Spectrosc. **169**, 329 (1995).
[33] A. Matzkin, Ch. Jungen, and S. C. Ross, Phys. Rev. A **62**, 062511 (2000).